Determining Aerodynamic Characteristics of an Unmanned Aerial Vehicle using a 3D Scanning Technique

Or D. Dantsker[*]

University of Illinois at Urbana–Champaign, Urbana, IL 61801

There are a variety of different methods to determine the aerodynamic characteristics of an aircraft. Generally, one could either: perform computational analysis on the theoretical model or test the physical aircraft and collect flight data using either on-board sensors or a motion capture system. A 3D scanning and analysis technique has been developed that allows the user to scan an uncharacterized aircraft of any size and output its aerodynamic coefficients, specifically the aircraft lift, drag, and moment curves as well as the associated stability derivatives. In order to demonstrate the method, a 62.5 in wingspan fixed-wing unmanned aerial vehicle (UAV) was 3D scanned. The point cloud yielded by the scan was then processed to produce detailed geometry of the aircraft and that geomerty was then input into an aerodynamics analysis tool, XFLR5. The analysis tool yielded the aircraft aerodynamics coefficients within the linear range.

Nomenclature

α	=	angle of attack
ARF	=	almost ready to fly
C_D	=	drag coefficient
C_L	=	lift coefficient
C_M	=	moment coefficient
C_{D_α}	=	drag curve slope
C_{L_α}	=	lift curve slope
C_{M_α}	=	moment curve slope
$COTS$	=	commercial off the shelf
CG	=	center of gravity
GPS	=	global positioning system
IMU	=	inertial measurement unit
Re	=	Reynolds number
RC	=	radio control
UAV	=	unmanned aerial vehicle

I. Introduction

There are a variety of different methods to determine the aerodynamic characteristics of an aircraft. In theory, one could measure the lift-to-drag ratio of an aircraft by commanding the aircraft into a glide and measuring the horizontal glide distance and dividing it by the vertical drop. However, to produce accurate measurements it is easier to use modern methods. Generally, one would either: perform computational analysis on the theoretical model or test the physical aircraft and collect flight or wind tunnel data.

A 3D scanning and analysis technique has been developed that allows the user to scan an uncharacterized aircraft and output its aerodynamic coefficients. Specifically the technique outputs with the aircraft lift, drag, and moment curves, along with the aircraft stability derivatives C_{L_α}, C_{D_α}, and C_{M_α}. This method was demonstrated using a 62.5 in wingspan fixed-wing unmanned aerial vehicle (UAV). The aircraft was 3D scanned, which yieled a point cloud, and

---

[*]Graduate Research Fellow, Department of Aerospace Engineering, AIAA Student Member. dantske1@illinois.edu

American Institute of Aeronautics and Astronautics

that point cloud was then processed to produce detailed geometry of the aircraft.The geomerty was then input into an aerodynamics analysis tool, XFLR5.[1] The tool yielded the aircraft aerodynamics coefficients within the linear range.

This paper will first briefly examine techniques used to determine the aerodynamic characteristics of an aircraft. The paper will then discuss the methodology used in 3D scanning technique. After that, demonstration of the technique on a 62.5 in wingspan fixed-wing UAV is given with the results. Finally, conclusions and future work is presented.

A.   Literature on Determining Aircraft Aerodynamic Characteristics

Most researchers these days determine the aerodynamic characteristics of an unmanned aircraft using two types of experimental methods. In both cases, they flight test the aircraft and either collect flight data using on-board sensors or externally using a motion capture system. There are a handful of examples for both methods.

On-board data collection requires an aircraft to carry a logging device and sensors, which increases the weight of the aircraft, and thereby limits what aircraft can be flight tested this way. Researchers at the University of Florida used a small outdoor aerobatic unmanned aircraft to investigate high angle-of-attack flight dynamics, which included stability issues that related to side slip[2] and wing rock;[3–5] the aircraft they used had all sensors and recording equipment on board. Researchers at NASA Ames Research Center and Langley Research Center have used a variety of instrumented aircraft to record flight data.[6–8] Further work has also occurred at the University of Kansas[9–13] and the University of Illinois.[14, 15]

In terms of using a motion capture system to capture aerodynamics data, state data is collected externally using motion capture systems set in indoor flying spaces with no wind. There is an inherent limitation that comes from the size of the flying space and the number of cameras available for that capture volume, so an aircraft must be below a certain size. This methods was used by researchers at the Georgia Institute of Technology, where a miniature indoor aerobatic aircraft was used to demonstrate a guidance controller for transitions into hovering state.[16] Similar work was done at the Massachusetts Institute of Technology[17] and Universit Laval.[18] Using a comparable motion capture system, researchers at the University of Illinois parameterized a micro, aerobatic aircraft to determine its aerodynamic characteristics including lift, drag, and moment curves over a wide flight regime.[19]

II.   Methodology

The 3D scanning and analysis technique allows a user to scan an uncharacterized aircraft and output its aerodynamic coefficients. The technique is separated into the following stages:

1. Assemble and prepare the aircraft

2. 3D scan the aircraft using a hand held scanner

3. Generate a 3D point cloud of the aircraft

4. Process the point cloud to give profile cuts of the aircraft

5. Use the profile cuts to generate a model in the aerodynamics analysis tool XFLR5

6. Output the aircraft polars and aerodynamic coefficients

The above list of stages gives a high-level description of the technique. More specifics can be found in Section III. In general, the technique outputs the aircraft lift, drag, and moment curves. Within the linear regime, it can generate the aircraft stability derivatives C_{L_α}, C_{D_α}, and C_{M_α}, which could be then used to create a basic linear aircraft model. Results in that regime, which would hopefully be comparable to those produced through flight testing, are shown in the following section and will be expanded in future work.

American Institute of Aeronautics and Astronautics

III. Demonstration

This section describes how 3D scanning and analysis technique was demonstrated on a 62.5 in wingspan fixed-wing UAV. The aicraft was scanned, the data from that scan was processed, and the aerodynamic characteristics computed.

A. 3D Scanning

The 3D scanning was performed using a ZCorporation ZScanner 800 self-postioning handheld 3D scanner,[20] see Figure 1. The scanner uses 3 high-speed, high-resolution CCD camera units and a laser projection unit to triangulate its position about the object while scanning it in real-time. The object is first prepared by randomly affixing retro-reflective dots to it with a spacing between the dots of between 20 to 100 mm. These dots allow the system to determine its position with relation to the object in 3D space. At any one time, the system must see at least 4 of these dots for positioning to occur. Creating these conditions may be difficult with certain objects depending on their geometric shape; for example a wing with a sharp leading edge. Then, once the dots are placed, the scanner is moved around the object with a set of crosshairs being projected onto the surface of the object. Depending on how the crosshairs reflect from the surface of the object, the camera captures the profile of laser lines projected onto the object at a rate of 25,000 times per second, allowing the scanner to accurately build a triangulated surface. During this process, the scanner's computer uses a triangulation software to automatically captures the geometry of the part and the position of the unit. With everything operating correctly, the scanner generates a polygon mesh in real-time. With sufficient scanning, a complete 3D surface is created, which can be output as a 3D point cloud of that surface.

Figure 1. ZCorporation ZScanner 800

American Institute of Aeronautics and Astronautics

A 62.5 in wingspan fixed-wing UAV based on Great Planes Avistar Elite[21] was used to demonstrate the technique. The same aircraft has previously been used to test a sensor data acquisition system.[22–24] The Avistar UAV is a 8.7 lb fixed-wing trainer-type model airplane and is equipped with an electric propulsion system that uses a AXI 4120/14 600 W motor,[25] a Castle Creation Phoenix ICE 75 Amp electronic speed controller,[26] and a Thunder Power 14.8 V, 5 Ah lithium polymer battery.[27] The model is actuated using Futaba S3004 ball-bearing standard-torque servos and is controlled by a 2.4 GHz spread spectrum receiver.[28] The radio control system is powered by an independent Castle Creations CC BEC regulator, which uses a Thunder Power 7.4 V, 450 mAh lithium polymer battery. The aircraft was instrumented with the sensor data acquisition system mentioned previously and associated sensors, which partially changed the external geometry of the aircraft; e.g. a gps receiver lies aft of the wing on top the fuselage, a pitot probe attached to the left wingtip, and there are additional linkages and control arms found throughout the aircraft. The completed flight-ready aircraft is shown in Figure 2, its physical specification are given in Table 1, and its airframe component specification are given in Table 2.

Figure 2. Flight-ready Great Planes Avistar Elite model aircraft.

American Institute of Aeronautics and Astronautics

Geometric Properties	
Overall Length	55.0 in (1395 mm)
Wing Span	62.5 in (1590 mm)
Wing Area	672 in^2 (43.3 dm^2)
Aspect Ratio	6.62
Inertial Properties	
Weight	
Empty (w/o Battery)	7.53 lb (3.415 kg)
4S LiPo Battery	1.17 lb (0.530 kg)
Gross Weight	8.70 lb (3.945 kg)
Wing Loading	29.8 oz/ft^2 (90.9 gr/dm^2)

Table 1. Great Planes Avistar Elite model aircraft physical specifications

Construction	Built-up balsa and plywood structure, aluminum wing tube, aluminum landing gear, abs canopy, and plastic film sheeted.
Flight Controls	
Controls	Aileron (2), elevator, rudder, throttle, and flaps (2)
Transmitter	Futaba T14MZ
Receiver	Futaba R6014HS
Servos	(6) Futaba S3004
Regulator Distribution	Castle Creations CC BEC
Receiver Battery	Thunder ProLite 20c 2S 7.4V 450 mAh
Propulsion	
Motor	AXI 4120/14 Outrunner
ESC	Castle Creation Phoenix ICE 75 Amp Brushless Speed Controller
Propeller	APC 13x8E
Motor Flight Pack	Thunder Power ProPower 30c 4S 14.8 V 5 Ah lithium polymer battery
Flight Time	10-20 min

Table 2. Great Planes Avistar Elite model aircraft airframe component specifications

The Avistar UAV and ZScanner 800 were brought into a large empty room that had a minimal amount of reflections when lit for scanning. This provided the best possible lighting for the 3D scanner and adequate room for the rotating the aircraft. The Avistar UAV was assembled - multiple views of the aircraft are given in Figures 3-6. In order to prepare the Avistar UAV for the scanning process, retro-reflective dots were placed on the exterior surface of the aircraft. Dots were placed randomly with the required spacing on the left half of the aircraft, along with the complete top and bottom surfaces of the fuselage and both sides of the vertical stabilizer - see Figures 7-8.

The Avistar UAV was 3D scanned using the ZScanner 800. The aircraft was rotated through a variety of angles to allow the scanner to project its crosshairs and view the aircraft geometry -see Figures 9-10. Screenshots of the scanning process, given in Figures 11-12, show many non-existant artifacts, which are probably the result of nearby objects used to hold the aircraft. Almost all of the artifacts were removed using ZCorporation's ZScan softare, which was provided with the scanner, and yielded a cleaner surface mesh model, as seen in Figures 13-16; it should be noted that there are holes found throughout the surface mesh, which are the result of the software being unable to interpolate the surface shape underneath certain dots. The final surface mesh was output from ZScan as a 3D point cloud.

American Institute of Aeronautics and Astronautics

Figure 3. Top view of assembled Avistar UAV.

Figure 4. Isometric view of assembled Avistar UAV.

Figure 5. Front view of assembled Avistar UAV.

Figure 6. Side view of assembled Avistar UAV.

Figure 7. View of Avistar UAV with retro-reflective dots.

Figure 8. View of Avistar UAV with retro-reflective dots with flash lighting.

American Institute of Aeronautics and Astronautics

Figure 9. Scanning the top of the Avistar UAV.
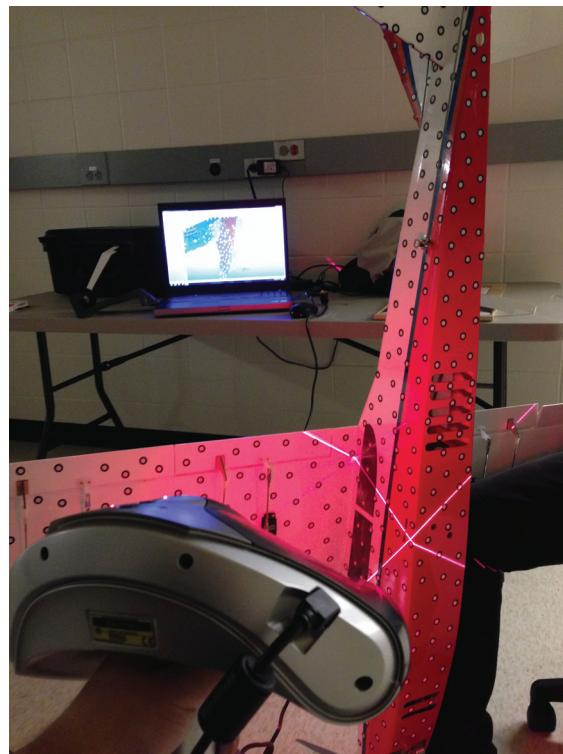
Figure 10. Scanning the bottom of the Avistar UAV.
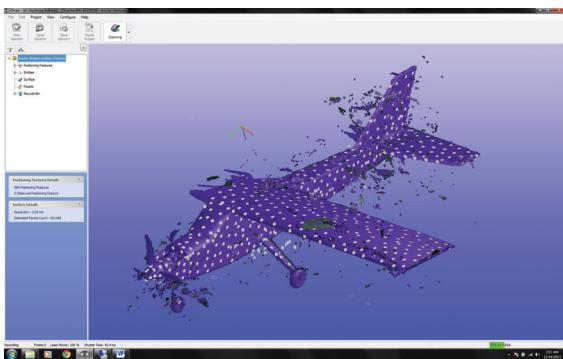
Figure 11. ZScan screenshot of the Avistar UAV from the top-left.
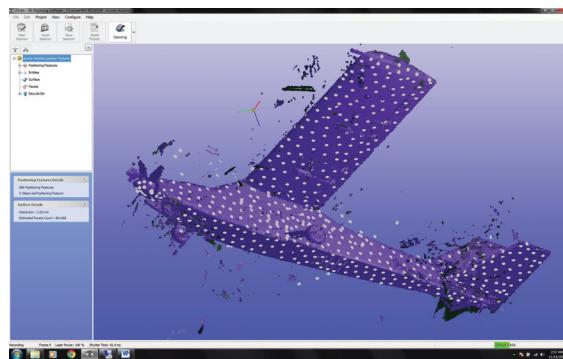
Figure 12. ZScan screenshot of the Avistar UAV from the bottom-left.

American Institute of Aeronautics and Astronautics
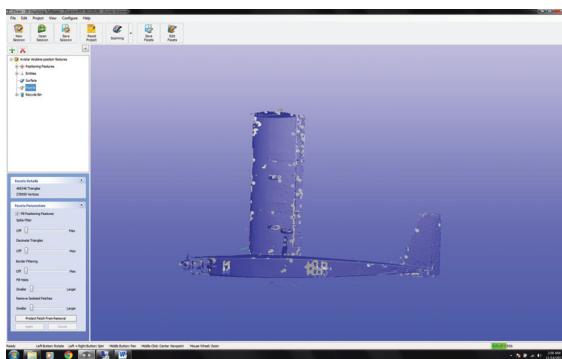
Figure 13. ZScan screenshot of the clean surface mesh model of the Avistar UAV from the bottom.
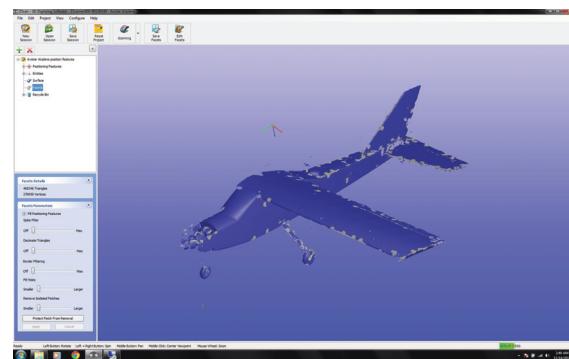
Figure 14. ZScan screenshot of the clean surface mesh model of the Avistar UAV from the top-left.
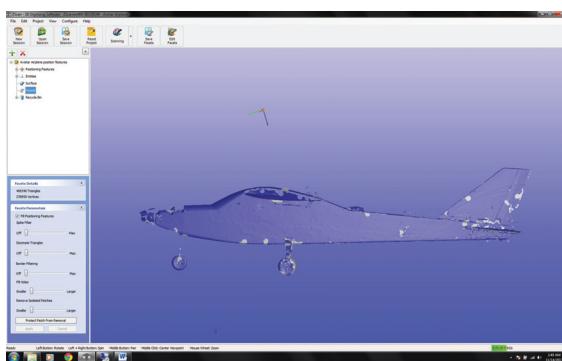
Figure 15. ZScan screenshot of the clean surface mesh model of the Avistar UAV from the left.
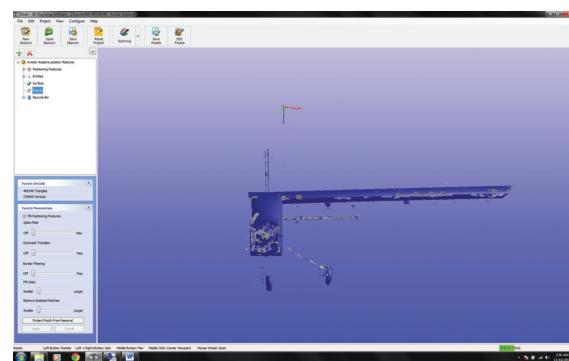
Figure 16. ZScan screenshot of the clean surface mesh model of the Avistar UAV from the front.

B. Data Processing

The 3D pointcloud output from the scanner was input into a MATLAB script called AirplaneScan for processing. AirplaneScan operates with a basic menu within the MATLAB command window. It can load the tab deliminated 3D pointcloud file contents into memory, clear its memory, save the pointcloud in memory to a file, plot the pointcloud in a 3-view and isometrically, translate the pointcloud in 3D space, rotate the pointcould about the axes, delete all points outside a given box, mirror the pointcloud about planes, and finally slice the pointcloud and output the points. See Figure 17 for a screenshot of the main menu of AirplaneScan.
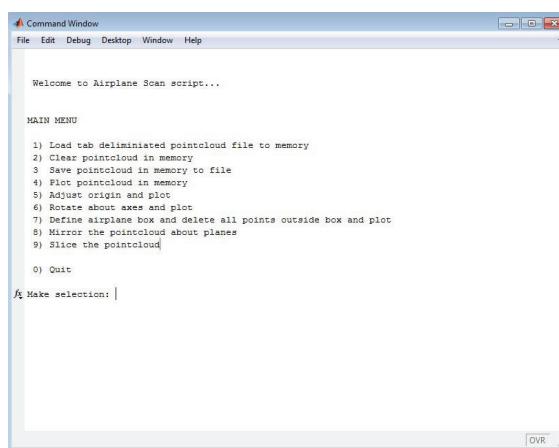
Figure 17. A screenshot of the AirplaneScan main menu.

American Institute of Aeronautics and Astronautics
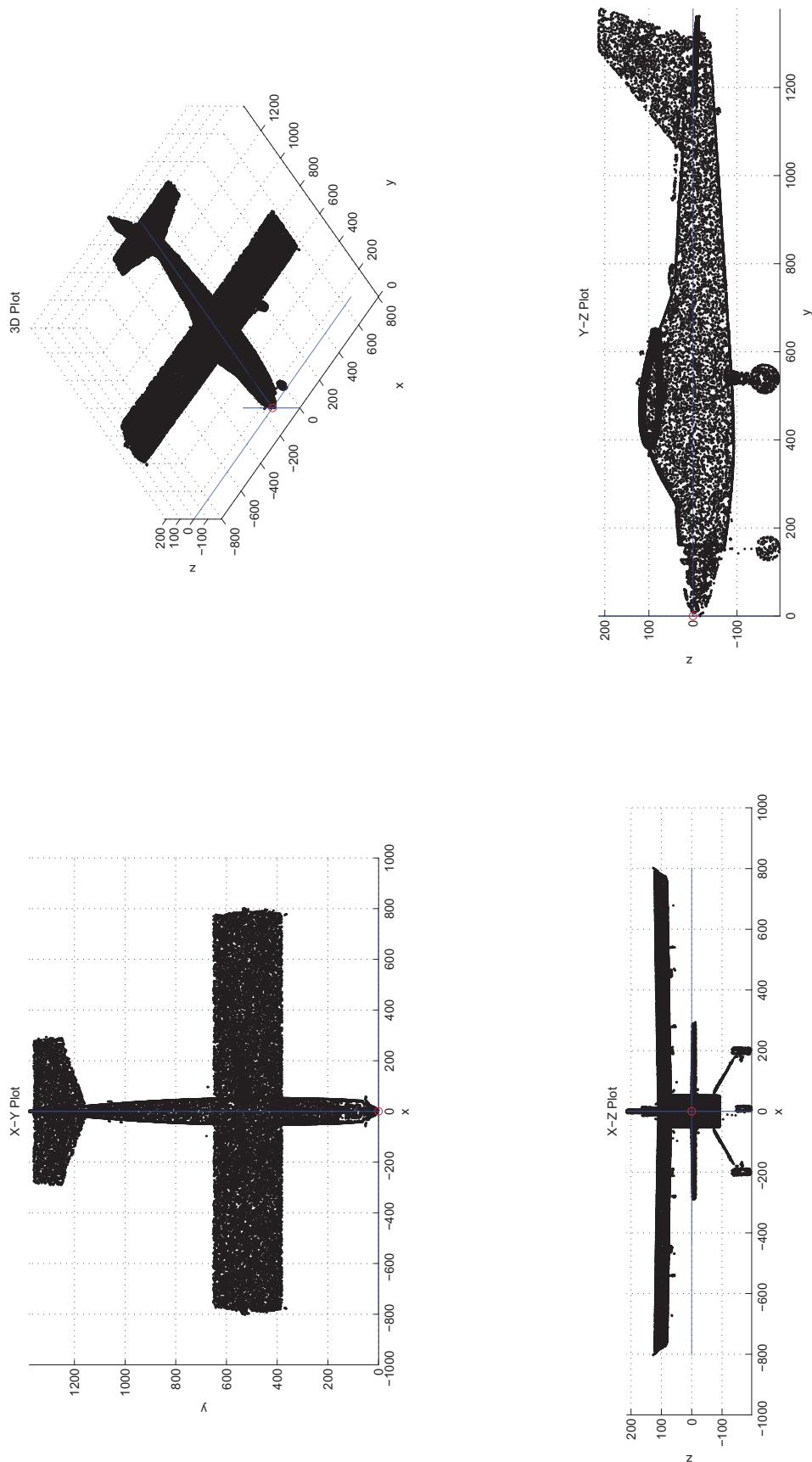
Figure 18. 3-view and isometric plots of the Avistar UAV scan after processing.

American Institute of Aeronautics and Astronautics
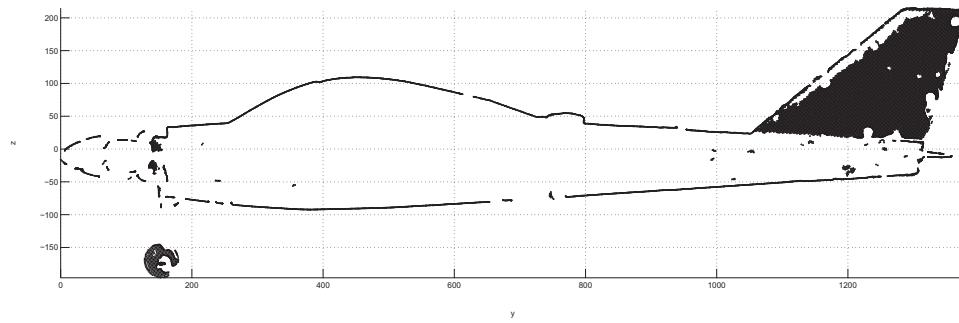
**Figure 19. Plot of Y-Z slice of the 3D scan point cloud between x=-5 and x=5.**
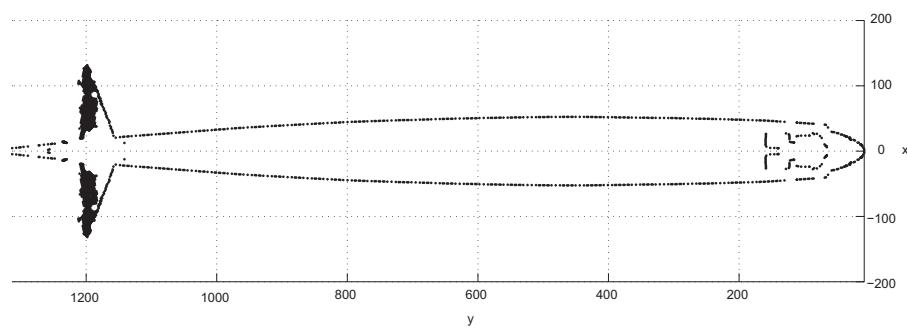
**Figure 20. Plot of X-Y slice of the 3D scan point cloud between z=0 and z=1.**
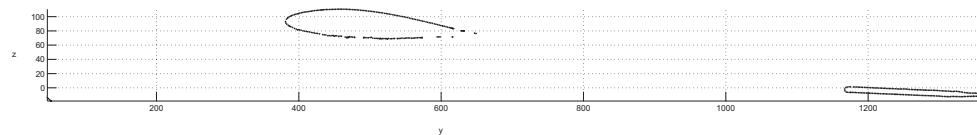
**Figure 21. Plot of Y-Z slice of the 3D scan point cloud between x=53 and x=55.**
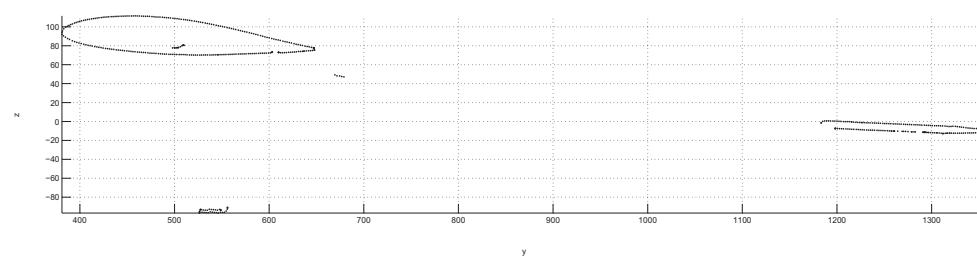
Figure 22. Plot of Y-Z slice of the 3D scan point cloud between x=98 and x=100.

American Institute of Aeronautics and Astronautics

Using AirplaneScan, the 3D scan pointcloud of the Avistar UAV was translated and rotated from its original skewed angle and location. The tip of the nosecone was placed at the origin with the x-axis toward the left, the y-axis out the tail, and the z-axis up; it should be noted that a non-standard coordinate system is used. The points on the right half of the airplane were discarded, and then the points on the left half were mirrored to the right with the exception of the nose gear which was not mirrored.The resulting processed 3D point cloud can be seen in a 3-view and isometric view in Figure 18. The processed point cloud was then sliced multiple times to yield the cross sections of the fuselage, wings, and tail sections; the points were plotted in Figures 19-22.

C. Computation and Results

The aircraft geometry generated by the 3D scan was implemented into the aerodynamics analysis tool, XFLR5. XFLR5 is based on XFOIL's[29] analysis capabilities and uses Lifting Line Theory, Vortex Lattice Method, and 3D Panel Method to generate results. The program has a few drawbacks including not being able to model fuselages well and only being able to use Vortex Lattice Method on aircraft (wings and tail surfaces) as opposed to just the wing where all three methods are available. This problem is well documented by the XFLR5 authors.[30]

The pointcloud slices generated by the AirplaneScan MATLAB script provided dimensions and coordinates for all of the flight surfaces. It is important to note that the wing has a constant airfoil throughout the span and the horizontal and vertical stabilizers each have continuously varying airfoils from root to tip. The coordinates of each airfoil produced were plotted in Figure 23. The dimensions of each flight surface and the airfoil locations can be found in Table 3. All of the information is given following XFLR5's coordinate axes with the x-axis towards the tail, the y-axis towards the right wing. and the z-axis up.
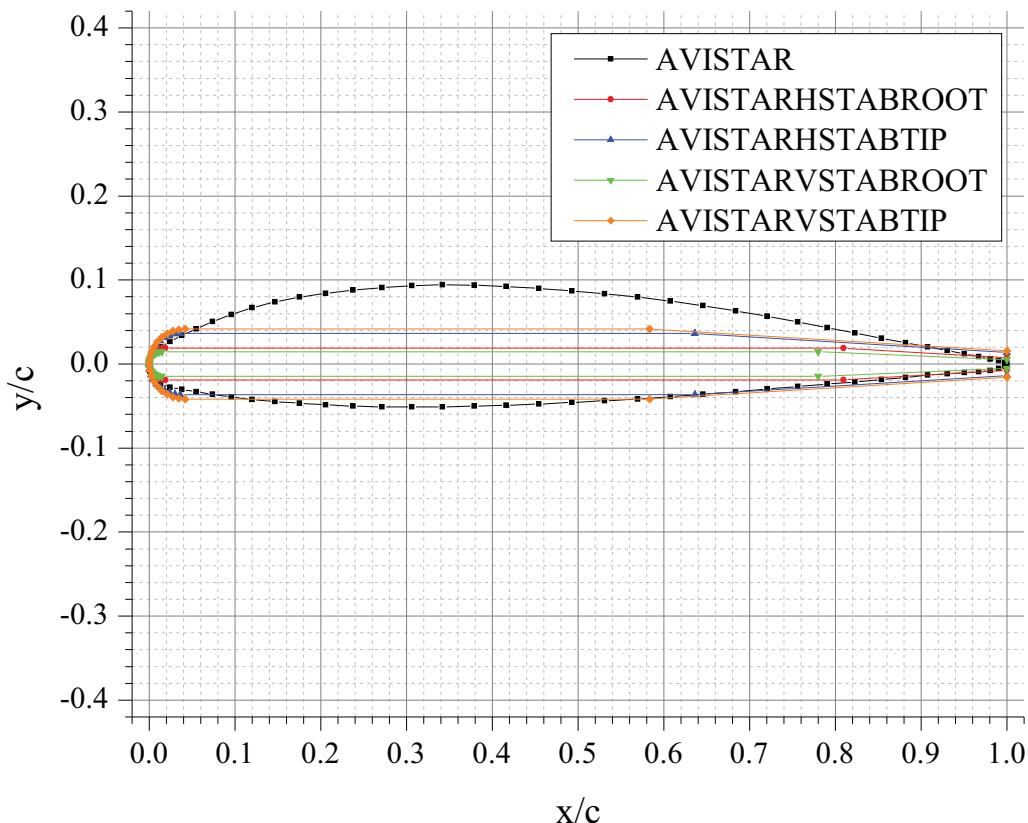

Figure 23. The airfoils used on the Avistar UAV.

American Institute of Aeronautics and Astronautics

Wing							
LE x pos	LE z pos	Incidence	y span pos	Chord	Offset	Dihedral	Airfoil
380.4 mm	95.5 mm	3.58 deg	0 mm	237.10 mm	0 mm	0.9 deg	AVISTAR
-	-	-	793.75 mm	237.10 mm	0 mm	-	AVISTAR
Horizontal Stabilizer							
LE x pos	LE z pos	Incidence	y span pos	Chord	Offset	Dihedral	Airfoil
1160 mm	-2.04 mm	2.36 deg	0 mm	210 mm	0 mm	0 deg	AVISTARHSTABROOT
-	-	-	291 mm	110 mm	100 mm	-	AVISTARHSTABTIP
Vertical Stabilizer							
LE x pos	LE z pos	Incidence	y span pos	Chord	Offset	Dihedral	Airfoil
1160 mm	17.96 mm	2.36 deg	0 mm	273 mm	-95 mm	0 deg	AVISTARVSTABROOT
-	-	-	200 mm	96 mm	133 mm	-	AVISTARVSTABTIP

Table 3. Avistar UAV flight surface specifications.

In order to verify the validity of the scan, the AVISTAR wing airfoil was compared to the coordinates for the AVISTAR airfoil found on the UIUC Airfoil Database.[31] Overall, there is minimal difference between the two with a slight lack of droop at the LE, as seen in Figure 24. There is similar droop in the UIUC LSATs[32] model tested, as can be seen in Figure 25, leading to the conclusion that the difference is a manufacturer deviation from the coordinates, as both the Avistar UAV and the LSATs AVISTAR airfoil tested were produced by Great Planes. Therefore, given the similarity between the scanned and database airfoils, the geometry generated from the 3D scan can be considered accurate.
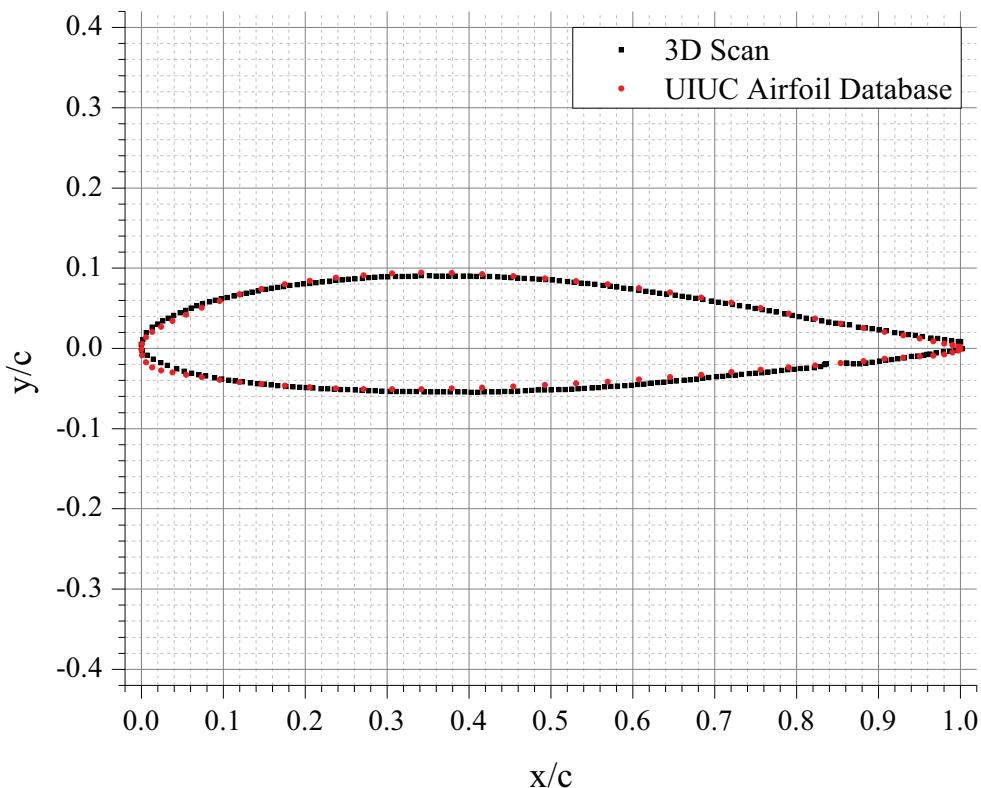

**Figure 24. The AVISTAR airfoil scan coordinate comparison.**
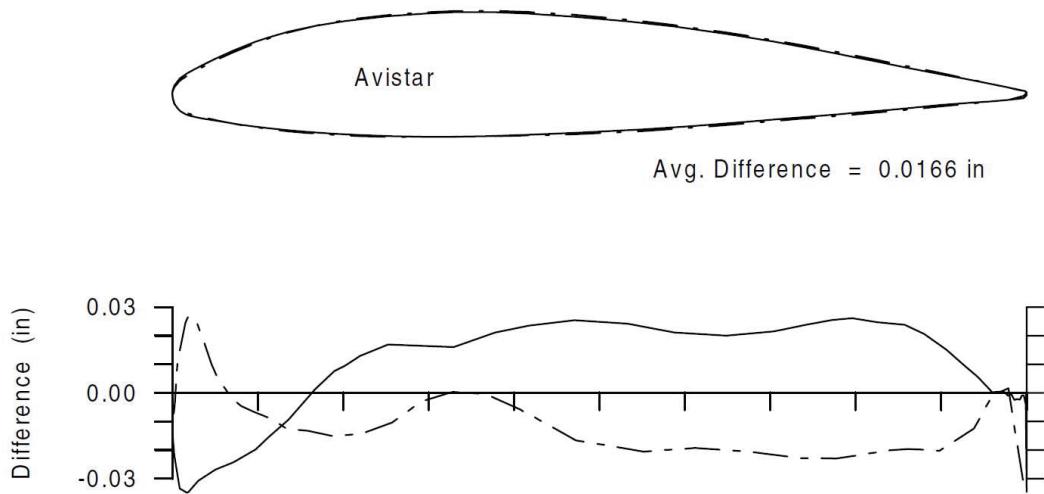
Figure 25. UIUC LSATs AVISTAR airfoil model comparisons: the top subfigure showing the true airfoil plotted with a solid line and the actual (tested) airfoil plotted with a dashed line, and the bottom subfigure showing the amount of deviation exhibited by the actual (tested) airfoil away from the true airfoil coordinates with the difference in the upper surface plotted with a solid line and the difference in the lower surface plotted with a dashed line. (taken from UIUC LSATs Volume 3[32]).

The airfoil coordinates and flight surface location were entered into XFLR5, and the resultant model can be seen in Figure 26. The fuselage was withheld from the aerodynamics model per recommendations provided in the documentation of XFLR5, as mentioned earlier. In order to test the aerodynamics model in XFLR5, each of the airfoils needed to be run for all possible Reynolds numbers and angles of attack. The Reynolds number was swept between 10,000 and 500,000 and the angle of attack was swept between -45 deg and 75 deg, to provide the greatest possible operating range for both the wing and stabilizers. XFLR5 was used to run Avistar aerodynamics model for flights speeds of 10 mph (4.5 m/s), 20 mph (8.9 m/s), 30 mph (13.4 m/s), 40 mph (17.9 m/s), 50 mph (22.4 m/s), and 60 mph (26.8 m/s) in viscous mode and it was also run in inviscid mode—see the polars in Figure 27.
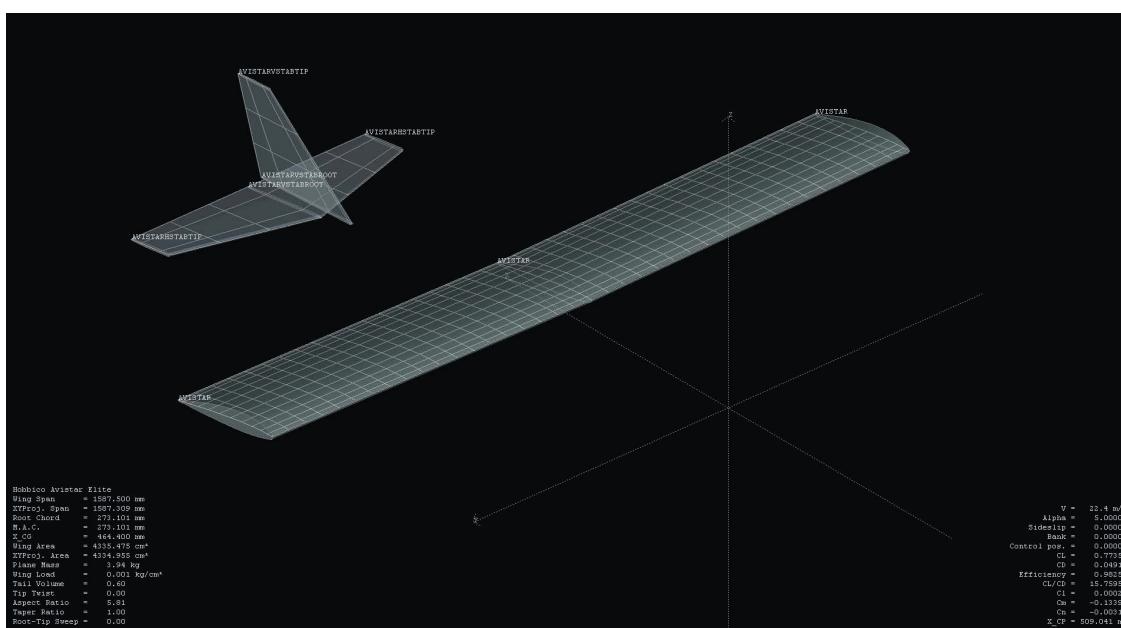

**Figure 26. XFLR5 aerodynamics model for the Avistar UAV**

American Institute of Aeronautics and Astronautics
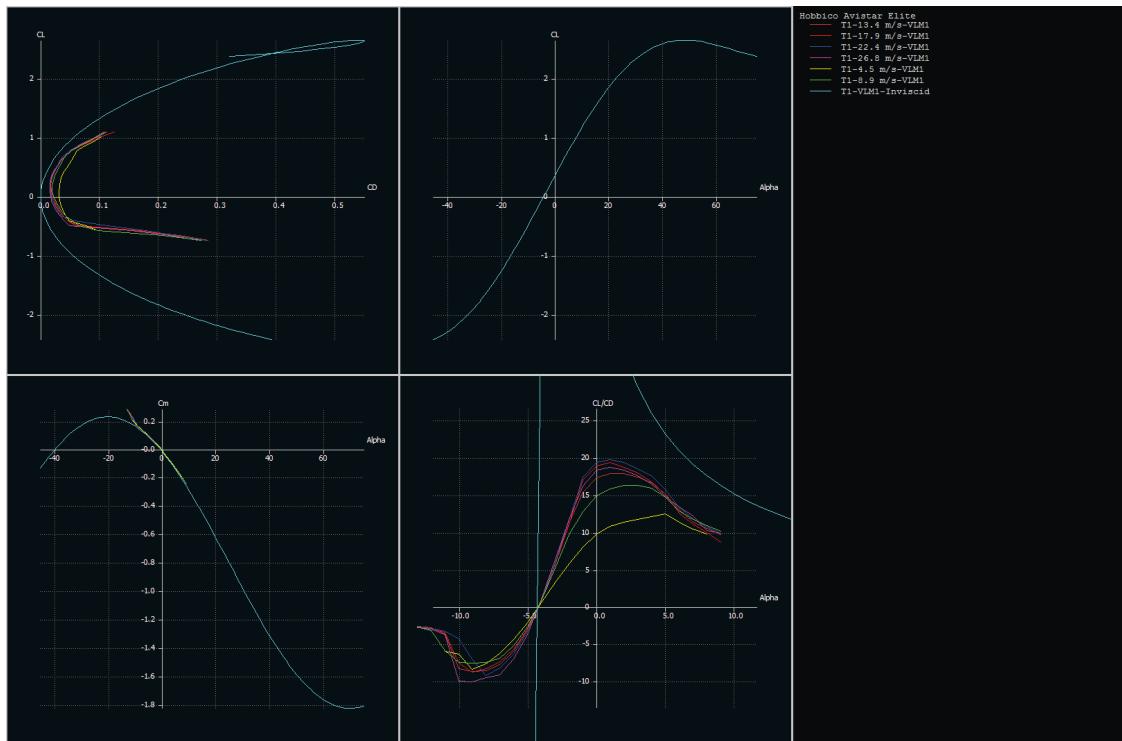
Figure 27. XFLR5 polars for the Avistar UAV
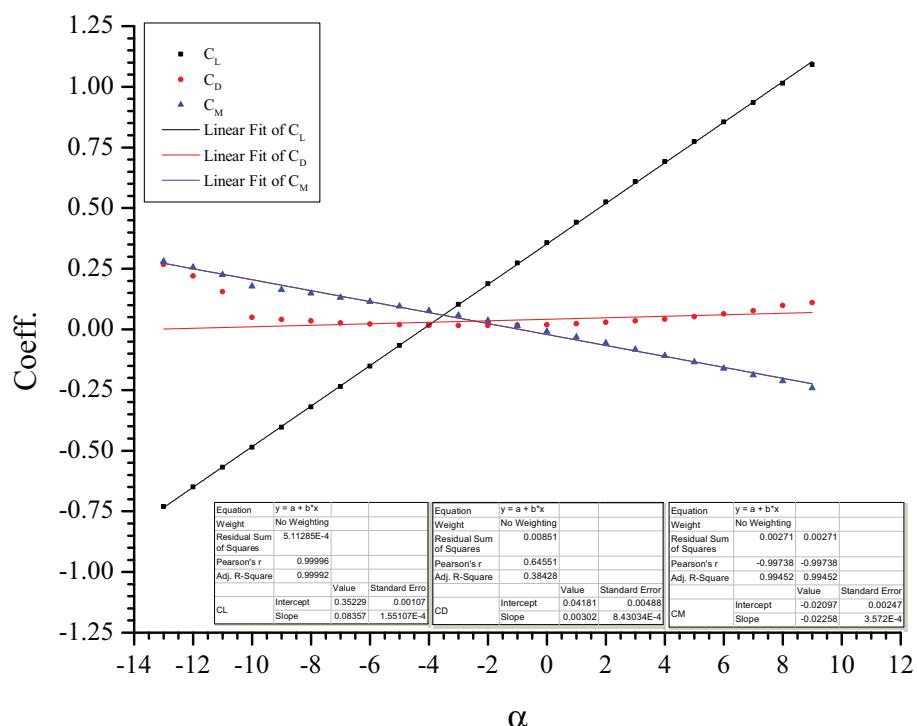
Figure 28. XFLR5 lift, drag, and moment coefficients against angle of attack for the Avistar UAV at 60 mph

American Institute of Aeronautics and Astronautics

XFLR5 was only able to produce viscous results within angles of attack of $\pm$ 10 deg. Beyond these angles, XFLR5 was unable to interpolate between the airfoil performance curves. As mentioned earlier, XFLR5 only allows for aircraft models to be run using Vortex Lattice Method, which produce results that are not quite viscous and therefore cannot capture stall. The inviscid method produced results for the entire angle of attack range, however, it failed to produce accurate drag predictions, due to the obvious lack of viscous drag, and accurate stall predictions.

From the viscous results, within angles of attack of $\pm$ 10 deg, the aircraft stability derivatives C_{L_α}, C_{D_α}, and C_{M_α} were be found. In Figure 28, the lift, drag, and moment coefficients for a flight speed of 60 mph were plotted against angle of attack, and these points are fitted linearly. The linear fittings, which were performed within the angle of attack range of $\pm$ 10 deg, produced slopes for each curve which are equal to the stability derivatives. It should be noted that this is not a standard method for calculating the drag stability derivative, however, since the standard method relies on knowing the Oswald efficiency factor, which is assumed to not be known a priori, we revert to using the linear fitting in a slightly parabolic range; the non-standard method for finding the drag term provides us a good first order approximation. The values of the stability derivatives produced are:

- $C_{L_\alpha} = 0.08357$

- $C_{D_\alpha} = 0.00302$

- $C_{M_\alpha} = -0.02258$

IV.   Conclusions and Future Work

The 3D scanning and analysis technique presented has shown some promise in producing aircraft lift, drag, and moment curves. The 3D scanning and point cloud processing method was able to produce detailed geometry of the aircraft, which in the case of the wing airfoil, was shown to match up with database coordinates. From the geometry produced, the lift, drag, and moment curves were found for the linear regime, which were then used to find the aircraft stability derivatives C_{L_α}, C_{D_α}, and C_{M_α}. The technique, however, fell short in producing the aircraft lift, drag, and moment curves for the entire flight regime—to stall. The problem encountered was the result of limitations inherent in the aerodynamics analysis tool used, XFLR5. In order to improve the range of reliable results, a different aerodynamics analysis tool would need to be used. Future work would also include comparing the 3D scanning coefficient curves to those found through flight testing.

Acknowledgments

References

[1]Andre Deperrois, "XFLR5," http://www.xflr5.com/, Accessed Dec. 2013.

[2]Perry, J., Mohamed, A., Johnson, B., and Lind, R., "Estimating Angle of Attack and Sideslip Under High Dynamics on Small UAVs," Proceedings of the ION-GNSS Conference, Savannah, Georgia, 2008.

[3]Johnson, B. and Lind, R., "High Angle-of-Attack Flight Dynamics of Small UAVs," AIAA Paper 2009-61, AIAA Aerospace Sciences Meeting, Orlando, Florida, Jan. 2009.

[4]Johnson, B. and Lind, R., "Characterizing Wing Rock with Variations in Size and Configuration of Vertical Tail," AIAA Paper 2009-6151, AIAA Atmospheric Flight Mechanics Conference, Chicago, Illinois, Aug. 2009.

[5]Johnson, B. and Lind, R., "Characterizing Wing Rock with Variations in Size and Configuration of Vertical Tail," *Journal of Aircraft*, Vol. 47, No. 2, 2010, pp. 567–576.

[6]Saha, B., Koshimoto, E., Quach, C. C., Hogge, E. F., Strom, T. H., Hill, B. L., Vazquez, S. L., and Goebel, K., "Battery Health Management System for Electric UAVs," IEEE Aerospace Conference, Big Sky, Montana, 2011.

[7]Ippolito, C., Yeh, Y. H., and Kaneshige, J., "Neural Adaptive Flight Control Testing on an Unmanned Experimental Aerial Vehicle," AIAA Paper 2007-2827, AIAA Infotech@Aerospace, Rohnert Park, California, May 2007.

[8]Jordan, T. L. and Bailey, R. M., "NASA Langley's AirSTAR Testbed: A Subscale Flight Test Capability for Flight Dynamics and Control System Experiments," AIAA Paper 2008-6660, AIAA Atmospheric Flight Mechanics Conference, Honolulu, Hawaii, Aug. 2008.

[9]Keshmiri, S., Leong, E., Jager, R., and Hale, R., "Modeling and Simulation of the Yak-54 Scaled Unmanned Aerial Vehicle Using Parameter and System Identification," AIAA Paper 2008-6900, AIAA Atmospheric Flight Mechanics Conference, Honolulu, Hawaii, Aug. 2008.

[10]Jones, V. A. and Keshmiri, S., "First Flight Risk Mitigation Related to Pilot Unfamiliarity with a New UAV Platform," AIAA Paper 2010-3489, AIAA Infotech@Aerospace, Atlanta, Georgia, June 2010.

[11]Lykins, R. and Keshmiri, S., "System Identification of a COTS Autopilot System Using Flight Test Data," AIAA Paper 2010-7648, AIAA Atmospheric Flight Mechanics Conference, Toronto, Ontario, Canada, Aug. 2010.

[12]Lykins, R. and Keshmiri, S., "Modal Analysis of 1/3-Scale Yak-54 Aircraft Through Simulation and Flight Testing," AIAA Paper 2011-6443, AIAA Atmospheric Flight Mechanics Conference, Portland, Oregon, Aug. 2011.

[13]Sebes, J., VanSkike, W., Williams, M., McCandless, S. E., Stastny, T., Worden, G., and Brunkhorst, N., "Flight Testing and Evaluation of the Structural Response to Flight Loads of a Small Scale Unmanned Aerial System," AIAA Paper 2012-2498, AIAA Infotech@Aerospace, Garden Grove, California, June 2012.

[14]Dantsker, O. D., Johnson, M. J., Selig, M. S., and Bretl, T. W., "Development of the UIUC Aero Testbed: A Large-Scale Unmanned Electric Aerobatic Aircraft for Aerodynamics Research," AIAA Paper 2013-2807, AIAA Applied Aerodynamics Conference, San Diego, California, June 2013.

[15]Ragheb, A. M., Dantsker, O. D., and Selig, M. S., "Stall/Spin Flight Testing with a Subscale Aerobatic Aircraft," AIAA Paper 2013-2806, AIAA Applied Aerodynamics Conference, San Diego, California, June 2013.

[16]Blauwe, H. D., Bayraktar, S., Feron, E., and Lokumcu, F., "Flight Modeling and Experimental Autonomous Hover Control of a Fixed Wing Mini-UAV at High Angle of Attack," AIAA Paper 2007-6818, AIAA Guidance, Navigation, and Control Conference, Hilton Head, South Carolina, Aug. 2007.

[17]Frank, A., McGrewy, J. S., Valentiz, M., Levinex, D., and How, J. P., "Hover, Transition, and Level Flight Control Design for a Single-Propeller Indoor Airplane," AIAA Paper 2007-6318, AIAA Guidance, Navigation, and Control Conference, Hilton Head, South Carolina, Aug. 2007.

[18]Bilodeau, P. R., Poulin, E., Gagnon, E., Wong, F., and Desbiens, A., "Control of a Hovering Mini Fixed Wing Aerial Vehicle," AIAA Paper 2009-5794, AIAA Guidance, Navigation and Control Conference, Chicago, Illinois, Aug. 2009.

[19]Uhlig, D., Sareen, A., Sukumar, P., Rao, A. H., and Selig, M. S., "Determining Aerodynamic Characteristics of a Micro Air Vehicle Using Motion Tracking," AIAA Paper 2010-8416, AIAA Guidance, Navigation, and Control Conference, Toronto, Ontario, Canada, Aug. 2010.

[20]ZCorporation, "The New ZScanner 800," www.zcorp.com/documents/182_ZScanner800-tearsheet-v05wb.pdf, Accessed Mar. 2013.

[21]Hobbico, Inc., "Great Planes Avistar Elite .46 Advanced Trainer RTF," http://www.greatplanes.com/airplanes/gpma1605.html, Accessed Oct. 2013.

[22]Mancuso, R., Dantsker, O. D., Caccamo, M., and Selig, M. S., "A Low-Power Architecture for High Frequency Sensor Acquisition in Many-DOF UAVs," Submitted to International Conference on Cyber-Physical Systems, Berlin, Germany, April 2014.

[23]Dantsker, O. D., Mancuso, R., Selig, M. S., and Caccamo, M., "High-Frequency Sensor Data Acquisition System (SDAC) for Flight Control and Aerodynamic Data Collection Research on Small to Mid-Sized UAVs," AIAA Paper 2014-2565, AIAA Applied Aerodynamics Conference, Atlanta, Georgia, June 2014.

[24]Dantsker, O. D., Mancuso, R., Caccamo, M., and Selig, M. S., "Robust Sensor Fusion for State Estimation on Agile Electric UAVs," Submitted to IEEE Real-Time Systems Symposium, Rome, Italy, Dec. 2014.

[25]Model motors s.r.o., "AXI 4120/14 GOLD LINE," http://www.modelmotors.cz/index.php?page=61&product=4120&serie=14&line=GOLD, Accessed Oct. 2013.

[26]Castle Creations, Inc., "Products for Flying," http://www.castlecreations.com/products/products_fly.html, Accessed Oct. 2013.

[27]Advanced Energy Tech, "Thunder Power RC," http://thunderpowerrc.com/, Accessed Nov. 2012.

[28]Hobbico, Inc., "Futaba Radio Control Systems and Accessories," http://futaba-rc.com/, Accessed Oct. 2013.

[29]Mark Drela, "XFLR5," http://web.mit.edu/drela/Public/web/xfoil/, Accessed Dec. 2013.

[30]Andre Deperrois, "F.A.Q : Why do I get the message "Point is out of the flight envelope ?"," http://www.xflr5.com/docs/Point_Out_Of_Flight_Envelope.pdf, Accessed Dec. 2013.

[31]UIUC Applied Aerodynamics Group, "UIUC Airfoil Coordinates Database," http://aerospace.illinois.edu/m-selig/ads/coord_database.html.

[32]UIUC Applied Aerodynamics Group, "UIUC Low-Speed Airfoil Tests (UIUC LSATs)," http://aerospace.illinois.edu/m-selig/uiuc_lsat.html.